Proceedings of the 17th World Congress
The International Federation of Automatic Control
Seoul, Korea, July 6-11, 2008

Towards Autonomous Fixed-Wing Unmanned Aerial Vehicle Landing: A Vision-Aided Inertial Navigation under Sensor Reconfiguration Scenario

Sungmoon Joo*, Khalid Al-Ali**
Corey Ippolito*, Yoo-Hsiu Yeh *****

**Department of Aeronautics and Astronautics, Stanford University, Stanford, CA, 94305 USA (Tel: 650-387-4715; e-mail:joosm@stanford.edu).*
***, ****Carnegie Mellon University-West Coast Campus, Moffet Field, CA 94035 USA (e-mail: alali@cmu.edu,yoohsiu.yeh@west.cmu.edu)*
**** Adaptive Control and Evolvable Systems Group, NASA Ames Research Center, Moffet Field, CA 94035 USA (e-mail:cippolito@mail.arc.nasa.gov)*

Abstract: While autonomous landing of unmanned aerial vehicles (UAVs) requires accurate position estimation, the standard inertial navigation unit (INU, the inertial measurement unit with a global positioning system (GPS)) provides relatively poor accuracy in altitude estimation. A common solution for this problem is to aid the INU with additional sensors and/or ground infrastructures, but the main hurdles to the approach are the limited payload of UAVs and extra cost involved. Dynamic sensor reconfiguration can be a good alternative by constructing a new sensor system utilizing available sensors around without adding new sensory equipment to UAVs. In this paper, a sensor reconfiguration scenario for autonomous fixed-wing UAV landing is considered and the resulting vision-aided inertial navigation system is investigated. This paper presents (i) a sensor fusion algorithm for a passive monocular camera and an INU based on the Extended Kalman Filter (EKF), and (ii) an object-detection vision algorithm using optical flow. The EKF is chosen to take care of the nonlinearities in the vision system, and the optical flow is used to robustly detect the UAV from noisy background. Pilot-controlled landing experiments on a NASA UAV platform and the filter simulations were performed to validate the feasibility of the proposed approach. Promising results were obtained showing 50%-80% error reduction in altitude estimation.

1. INTRODUCTION

1.1 Background & Motivation

Recent advances in distributed wireless technologies are opening the door to new methods of control reconfiguration utilizing remote avionics, actuation, and sensing. These dynamic reconfiguration networks would allow for the instantaneous restructuring of coordinated control system topologies in a group of vehicles that could include delocalized sensor, actuator, and controller components. They provide fault-tolerance to a wider class of vehicle system failures that conventional approaches are ill-equipped or unable to handle. Control systems in these dynamic networks could conceivably be capable of instantaneous polymorphic change - that is, the instantaneous and fundamental restructuring of the controller form and function. A polymorphic control architecture could provide on-the-fly reconfiguration to optimize a controller topology given radical changes in the environment (Ippolito et al., 2007).

Consider an autonomous fixed-wing UAV landing as an example of such a sensor reconfiguration. Autonomous aircraft landing requires accurate control over the flight trajectory in the presence of wind and gusts near the ground. In some cases, automation of UAV landing requires measurement of altitude above ground level (AGL) with an accuracy of 0.2m (Tomczyk et al., 1999). However, the current standard GPS system only provides a position accuracy of approximately 10m (with 95% confidence) in the horizontal direction and 15m (with 95% confidence) in the vertical direction; in addition, GPS can be easily compromised in some hostile environments (e.g. by jamming). Thus the standard INU alone is not good enough (particularly altitude AGL estimation) for an autonomous fixed-wing UAV landing system. Even though differential GPS (DGPS) or other onboard sensors (e.g. altimeter or range finder) are available for more accurate landing aid, their complexity, cost, limited payload capacity of UAVs, and the need of additional ground infrastructure make them prohibitive solutions for small/mid-sized fixed-wing UAVs. If there are reconfigurable external aiding sensors around (e.g. autonomous ground rovers with communication, GPS, and vision system), on-the-fly sensor reconfiguration can provide a more accurate position estimate to accomplish successful autonomous fixed-wing UAV landing without additional onboard/ground equipment installation.

1.2 Related Work

Most of the work done regarding autonomous landing of UAVs has focused on rotary wing aircraft and several of them have demonstrated reliable performance (Hubbard et al.,

2007). Vision-only or vision-based approaches are common in the previous studies, but they usually require a known/structured marker (Proctor et al., 2005), and, as mentioned above, non-vision based approaches use beacons, DGPS, or range finders which require additional onboard hardware and/or ground infrastructure. For fixed-wing UAVs, Pisanich et al. (2002) have demonstrated an autonomous landing capability. They use the waypoint following approach in which the UAV descends blindly toward a waypoint below the ground level with low speed until it touches the ground, in which it is hard to guarantee safe landings. Portable radar units and airborne transponders are adapted by many military UAVs providing accurate guidance for landing, but those systems are not practical for small/mid-sized UAVs (Quigley et al., 2005).

As for vision-based approaches for fixed-wing UAVs, optical flow has been used as an autonomous landing aid. Green et al. (2003) have used optical flow for autonomous landing of miniature UAVs. They were able to decrease forward speed in proportion to altitude by gradually throttling down the motor while keeping the optic flow on the landing surface constant. Barber et al. (2005) proposed a similar method for altitude AGL estimation using optical flow and barometric altimeter data. These approaches use separate miniature optical flow sensors for optical flow detection. Recently, Schultz et al. (2007) proposed a vision-based fixed-wing UAV landing system using a known marker and showed the feasibility of vision-aided precision fixed-wing UAV landings.

The limitations or weaknesses of most previous vision-based approaches can be summarized as follows: (i) a structured target is needed, which is unrealistic for landings in unstructured environments, and (ii) additional sensors are used in the case of optical flow applications.

1.3 Contributions

In this work we consider a sensor reconfiguration scenario for autonomous fixed-wing UAV landing, and present a position estimation system under the scenario, which consists of (i) a robust moving object detection algorithm using optical flow from a monocular camera, and (ii) an EKF based vision-aided position estimator without using a structured target. We used a NASA Exploration Aerial Vehicle (EAV) platform and a NASA MAX rover to verify the feasibility and performance of the proposed system for autonomous fixed-wing UAV landing.

2. VISION AIDED FIXED-WING UAV LANDING

2.1 Fixed-Wing Aircraft Landing Procedure

The typical aircraft landing procedure has three phases: approach, glideslope, and flare (Cohen *et al*., 1995). Fig.1 depicts the landing procedure. In the approach phase, the aircraft slows down to the reference approach speed and descends from cruising altitude towards a lower altitude. The glideslope phase starts when the aircraft finally stabilizes at a constant speed and rate of descent. During the glideslope phase, the aircraft should keep the flight path angle at -2.5 ~ -3.0 degrees and be descending towards an aiming point. When the aircraft reaches a prescribed flare altitude, the flare phase is initiated and the aircraft's attitude is changed from nose down to nose up. In the flare phase, the aircraft keeps a low attitude and gradually descends to a final altitude. At the final altitude, the aircraft flies level just above the runway and decelerates until touchdown point.

2.2 Sensor Reconfiguration Scenario for UAV Landing

The scenario consists of a fixed-wing UAV and a ground rover. The UAV has an IMU/GPS suite for navigation and a radio modem for communication. The rover equipped with a camera and a radio modem was deployed beforehand for some missions such as foreign object debris (FOD) detection and runway maintenance. When the UAV approaches to land, some performance metric will realize that the altitude and/or side-track error is too high, and will seek to hijack available ground-based sensors doing lower-priority functions. The vision sensor will be found from the rover, and the control systems on both the UAV and the rover will be reconfigured to form several distributed control loops on both systems. The UAV sends its state information packet (including position and velocity estimates) to the rover through the communication link. The rover uses the information to point its camera towards the UAV and initialize the vision system. Once the vision system detects the UAV, the rover sends relative bearing information and rover's position information back to the UAV. The UAV feeds the relative bearing and rover's position information into a position estimator to get better position estimates while executing a precise autonomous landing (Fig.2).

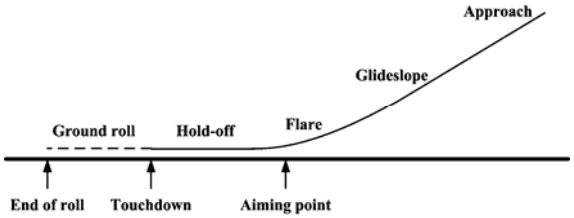

Fig. 1. Typical Aircraft Landing Procedure

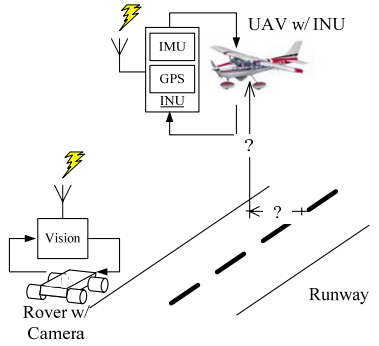

Fig. 2. Autonomous Landing Scenario Using Sensor Reconfiguration

2.3 System Description

The block diagram in Fig. 3 describes the sensor reconfiguration for autonomous landing. The position estimator can locate either in the UAV or in the rover.

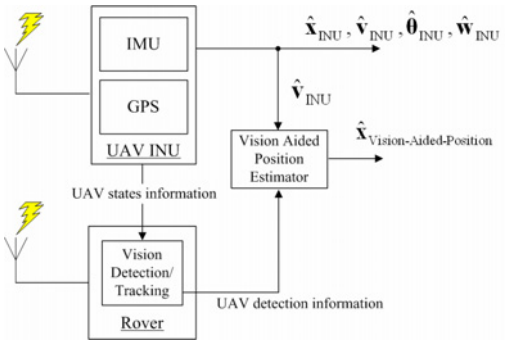

Fig. 3. UAV-Rover Sensor Reconfiguration Schematic

3. OPTICAL FLOW FOR UAV DETECTION

Detecting a UAV in the sky using a vision system is a challenging problem because the UAV appears as a small object, the lighting condition is uncontrollable, and background (e.g. clouds) can easily hinder the detection. In such cases, simple static object detection techniques like edge detection and background subtraction easily break. The use of optical flow estimation can increase the robustness in the vision system by detecting the apparent motion of the UAV.

3.1 Optical flow

The relative motion of objects and the view generates optical flow. Horn & Schunck (1981) defined optical flow as "the distribution of apparent velocities of motion of brightness patterns in an image." Mathematically, optical flow can be formulated as the inverse problem of estimating motion in an image sequence without tracking an object, which enables us to detect a moving UAV robustly.

3.2 OpticalFlowEsimation : Horn & Schunck's Method

The Horn & Schunck method (Horn & Schunck, 1981) is one of the most popular and benchmarked methods. Even though the method involves some errors in the estimation, it is chosen here because (i) the algorithm is simple, and (ii) the convergence property has been proven (Mitchie et al., 2004). The accuracy of optical flow estimation is not critical in the motion detection. In this section, Horn & Schunck's method is briefly introduced.

1) Assumptions

For convenience and simplicity, Horn & Schunck (1981) make the following assumptions:

A.1 The object being imaged is a flat surface.

A.2 The illumination on the image is constant and uniform.

A.3 The reflectance of the object varies smoothly and has no spatial discontinuities.

These assumptions also assure that the image brightness or intensity is differentiable (Horn & Schunck, 1981).

The assumptions A.1 and A.2 are not true in our application. The UAV, however, will appear as a flat object in the far distance. If there is intensity variation with time introduced due to illumination change, it will appear as a non-zero optical flow but that will not hinder the UAV detection.

2) Constraints

To relate the change in image brightness at a particular point to the motion of the brightness pattern, two constraints are established: (i) constant brightness constraint, and (ii) smoothness constraint.

C.1 Constant brightness constraint:

This constraint is an assumption that the intensity (E) at a particular point in an object does not change over time, i.e.:

$$\begin{aligned}\frac{dE}{dt} &= \frac{\partial E}{\partial x}\frac{dx}{dt} + \frac{\partial E}{\partial y}\frac{dy}{dt} + \frac{\partial E}{\partial t} \\ &= \frac{\partial E}{\partial x}u + \frac{\partial E}{\partial y}v + \frac{\partial E}{\partial t} \\ &= 0\end{aligned} \tag{1}$$

However, the constraint only gives information along the intensity gradient, the so-called aperture problem, and the flow velocity cannot be uniquely determined without an additional constraint for smoothness.

C.2 Smoothness constraint:

The brightness patterns in the image are assumed to vary smoothly and Horn & Schunck implemented this constraint by minimization of the square of the magnitude of the velocity:

$$\begin{aligned}\varepsilon_B &= E_x u + E_y v + E_t \\ \varepsilon_S^2 &= \left(\frac{\partial u}{\partial x}\right)^2 + \left(\frac{\partial u}{\partial y}\right)^2 + \left(\frac{\partial v}{\partial x}\right)^2 + \left(\frac{\partial v}{\partial y}\right)^2\end{aligned} \tag{2}$$

3) Algorithm

The optical flow (u and v) is found by minimization of both the error in the brightness equation and the measure of the smoothness constraint in (2). The total error to be minimized is defined by :

$$\varepsilon = \iint \alpha^2 \varepsilon_S^2 + \varepsilon_B^2 dxdy \tag{3}$$

4) Iterative solution

Since a direct solution to the constrained minimization is computationally very costly, an iterative solution is suggested :

$$\begin{aligned}u^{k+1} &= \bar{u}^k - E_x[E_x\bar{u}^k + E_y\bar{v}^k + E_t]/(\alpha^2 + E_x^2 + E_y^2) \\ v^{k+1} &= \bar{v}^k - E_y[E_x\bar{u}^k + E_y\bar{v}^k + E_t]/(\alpha^2 + E_x^2 + E_y^2)\end{aligned} \tag{4}$$

3.3 Hybrid Detection Algorithm

Using the position and velocity information from the UAV's INU, an approximate position of the UAV and an approximate value of the mean of optical flow is calculated. Then a small region of interest (ROI) is defined around the UAV position estimate. When the optical flow is expected to be over a threshold value, the optical flow estimation algorithm is

applied to the ROI. Otherwise a generic object detection algorithm can be applied.

4. POSITION ESTIMATOR

An EKF is designed and implemented to accommodate the nonlinear vision measurement (Brown *et al*., 1997, Grewal *et al*., 2001).

4.1 Coordinate systems

Three coordinate systems are considered : (i) North-East-Down (NED) coordinate for UAV and rover position reference, (ii) camera coordinate, attached to the camera in the rover, and (iii) image coordinate, attached to the camera coordinate.

The coordinate transformation between NED coordinate system and the camera coordinate system is defined by translation T, and Euler angles: yaw(ψ), pitch(θ), and roll(ϕ).

$$\begin{bmatrix} \tilde{\mathbf{X}}^C \\ \tilde{\mathbf{Y}}^C \\ \tilde{\mathbf{Z}}^C \end{bmatrix} = \mathbf{R}(X'',\phi)\mathbf{R}(Y',\theta)\mathbf{R}(Z,\psi) \begin{bmatrix} x_N - T_N \\ x_E - T_E \\ x_D - T_D \end{bmatrix} \tag{5}$$

where (T_N, T_E, T_D) is the rover(camera) position, (x_N, x_E, x_D) is the UAV position, and $(\tilde{\mathbf{X}}^C, \tilde{\mathbf{Y}}^C, \tilde{\mathbf{Z}}^C)$ is the camera coordinate. For simplicity, it is assumed that the runway is level and therefore the camera roll angle is zero.

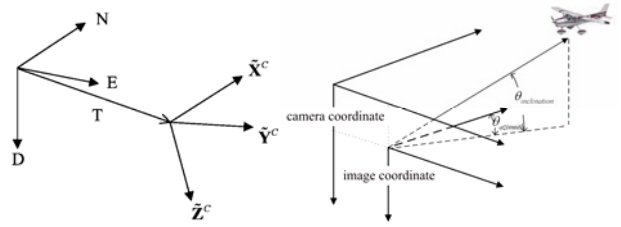

Fig. 4. Coordinate Systems

4.2 System Model

The system is described by a discrete linear dynamic equation with a time interval of Δt. The input is the velocity estimate from the inertial navigation unit.

$$\mathbf{x}_k = \mathbf{f}_{k-1}(\mathbf{x}_{k-1}, \mathbf{u}_{k-1}) + \mathbf{w}_{k-1} \tag{6}$$

where $\mathbf{x} = (x_N, x_E, x_D)$, $\mathbf{f}_{k-1} = \mathbf{F}_{k-1}\mathbf{x}_{k-1} + \mathbf{B}_{k-1}\mathbf{u}_{k-1}$, $\mathbf{F}_{k-1} = \mathbf{I}_{3\times 3}$, $\mathbf{B}_{k-1} = \Delta t \mathbf{I}_{3\times 3}$, and $\mathbf{w}_{k-1}$ is system noise.

4.3 Sensor Models

The camera measures two relative bearings: the inclination and azimuth in the camera coordinate. Note that the measurement is highly nonlinear.

$$\mathbf{z}_k = \mathbf{g}_k(\mathbf{x}_k) + \mathbf{v}_k \tag{7}$$

where $\mathbf{g}_k(\mathbf{x}_k) = \left[\tilde{\mathbf{Y}}_k^C / \tilde{\mathbf{X}}_k^C, \tilde{\mathbf{Z}}_k^C / \tilde{\mathbf{X}}_k^C\right]^T = \left[\tan(\theta_{inclination}), \tan(\theta_{azimuth})\right]^T$, and $\mathbf{v}_k$ is measurement noise.

4.4 Implementation of Estimator

The EKF filter implementation steps are as follows:

Step 0. Initialize the filter using $\hat{\mathbf{x}}(t_0)_{\text{INU}}$, $\mathbf{P}(t_0)$.

Step 1. Compute the predicted state estimate

$$\hat{\mathbf{x}}_k(-) = \mathbf{f}_{k-1}(\hat{\mathbf{x}}_{k-1}(+), \mathbf{u}_{k-1})$$

Step 2. Compute the predicted measurement

$$\hat{\mathbf{z}}_k = \mathbf{g}_k(\hat{\mathbf{x}}_k(-))$$

Step 3. Compute linear approximation equations

- System equation

$$\mathbf{F}_{k-1} = \partial \mathbf{f}_{k-1} / \partial \mathbf{x} \,|_{\mathbf{x}=\hat{\mathbf{x}}_{k-1}(+)} = \mathbf{I}_{3\times 3}$$

- Measurement equation

$$\mathbf{G}_k = \left.\frac{\partial \mathbf{g}_k}{\partial \mathbf{x}}\right|_{\mathbf{x}=\hat{\mathbf{x}}_k(-)} = \left.\begin{bmatrix} \partial \mathbf{g}_{1,k}/\partial x_N & \partial \mathbf{g}_{1,k}/\partial x_E & \partial \mathbf{g}_{1,k}/\partial x_D \\ \partial \mathbf{g}_{2,k}/\partial x_N & \partial \mathbf{g}_{2,k}/\partial x_E & \partial \mathbf{g}_{2,k}/\partial x_D \end{bmatrix}\right|_{\mathbf{x}=\hat{\mathbf{x}}_k(-)}$$

Step 4. Compute the a priori covariance matrix

$$\mathbf{P}_k(-) = \mathbf{F}_{k-1}\mathbf{P}_{k-1}(+)\mathbf{F}_{k-1}^T + \mathbf{Q}_{k-1}$$

Step 5. Compute the Kalman filter gain

$$\mathbf{K}_k = \mathbf{P}_k(-)\mathbf{G}_k^T\left(\mathbf{G}_k\mathbf{P}_k(-)\mathbf{G}_k^T + \mathbf{R}_k\right)^{-1}$$

Step 6. Update the state estimate with measurement residual

$$\hat{\mathbf{x}}_k(+) = \hat{\mathbf{x}}_k(-) + \mathbf{K}_k(\mathbf{z}_k - \hat{\mathbf{z}}_k)$$

Step 7. Compute the a posteriori covariance matrix

$$\mathbf{P}_k(+) = (\mathbf{I} - \mathbf{K}_k\mathbf{G}_k)\mathbf{P}_k(-)$$

5. EXPERIMENTS & ESTIMATOR SIMULATIONS

A series of flight tests were conducted to verify the performance of the proposed vision aided position filtering for an autonomous UAV landing system. This section presents the results of the experiments along with the estimator simulations. As the UAV approaches for landing, the rover's vision system detects the UAV and sends the measurements to the UAV. The position estimator on the UAV is initiated by the cue from the rover. The experiments were pilot-controlled and open-loop.

5.1 Experimental Hardware

1) NASA Exploration Aerial Vehicle (EAV)

NASA Ames Research Center (ARC) has developed in-house capabilities for flight validation on a smaller scale, with the focus on reduced costs associated with performing flight test experiments on a real vehicle system. The EAV project currently fields three aircrafts based on the Hangar 9 Cessna 182 Skylane 95" ARF platform, which is modelled after the 2000 version of a Cessna 182 at one quarter-scale. The

modified Hangar 9 Cessna aircraft has proven to be a reliable platform for flight testing.

Table 1. EAV Specification

Wing Span/ Length	2.4 m / 1.9m
Flying Weight	8.22 kg(Empty), 10.52 kg(Full)
Max Payload Weight	4.5 kg
Cruise Speed	23 m/s
Operations Ceiling	152m (flight field restrictions)
Engine/ Type	Zenoah G-38 / 2-Stroke Gas/Oil
Primary CPU	Diamond Athena 660MHz/128MB RAM
Sensors	High fidelity INU, WAAS-enabled GPS, angle of attack, sideslip, airspeed and altitude
Communications	• 72Mhz Receiver (Pilot/Safety Control) • 900Mhz Transceiver (Data Communications) • 2.4GHz Transmitter (Data/Video Downlink)

2) NASA MAX rover

A NASA MAX 5A rover was used as the camera platform. The rover is designed and built as a testbed for polymorphic control system by Carnegie Mellon University and is now commercially available (www.senseta.com). The rover's extensive IO capability and rich sensor suite, including camera, GPS, and LIDAR make it a perfect platform for the sensor reconfiguration scenario.

Table 2. MAX 5A rover Specification

Dimension / Weight	0.45m x 0.38m x 0.48m / 9.5 kg
Speed	~6m/s
Primary CPU	1.6 GH Pentium M
Communications	802.11g (2.4 GH) & 900 Mhz Radio Modem
Sensors	Stereo Camera Pair(640x480) Sonar Ranger Finders(up to 10), LIDARs (up to 6) High fidelity INU(with DGPS) sensor suite
Actuation	Pan and Tilt Camera Head Four-wheel Drive w/Double-Ackerman Steering

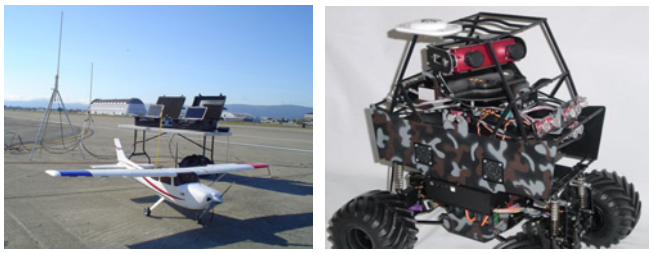

Fig. 5. NASA EAV and MAX rover

5.2 Results

During the flight tests, a number of landing maneuvers were performed. These maneuvers were recorded by both the avionics on the EAV and the rover. The camera on the rover also recorded the maneuvers.

Fig. 6 ~ Fig. 8 show the altitude AGL profile of some of the landing maneuvers. Fig. 6 is a bumpy landing and Fig. 7 and 8 are soft landings. Since we do not have absolute altitude AGL measurements, the videos and vertical speed records are used to verify the actual touchdown. It turned out that the vertical speed is a good indicator of touchdowns. The performance of the vision aided position estimator is clearly shown in the close-up view of touchdowns (Fig. 6-2, 7-2, 8-2). While the nominal INU gives 3.5~7m error in altitude AGL, the vision aided position estimator has less than 1.5m error. There are still delays of about 2 seconds in the altitude estimates of the vision aided position estimator. Those are believed to be due to (i) uncertainties in the rover position and camera angles, (ii) measurement delay from the communication and vision processing , and (iii) weak observability of the monocular camera.

Even though we do not have absolute measurements for lateral positions, it is expected that the vision aided position estimator has more accurate position estimates than the nominal INU. Fig. 9 is an example of 3D position estimation.

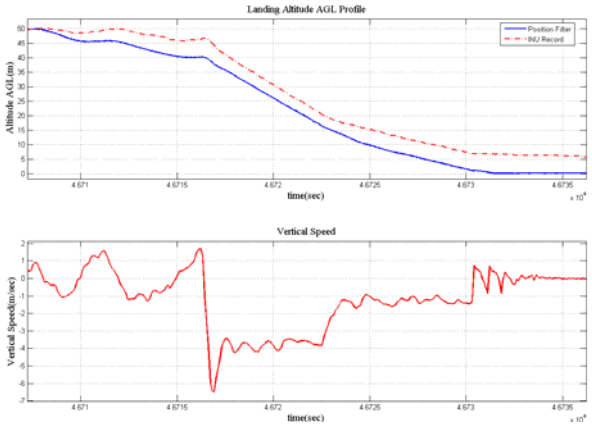

Fig. 6-1. Landing #1

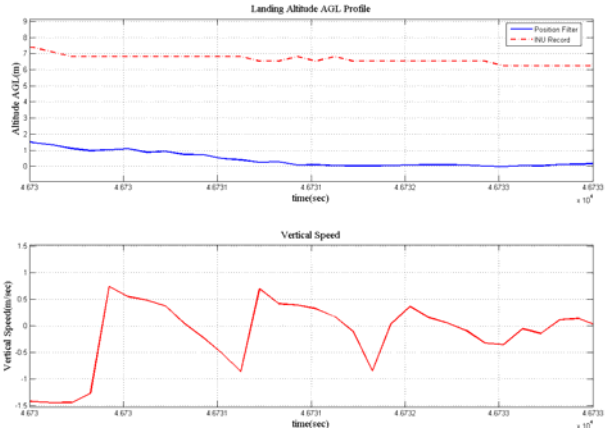

Fig. 6-2. Landing #1 : Close-up View of Touchdown

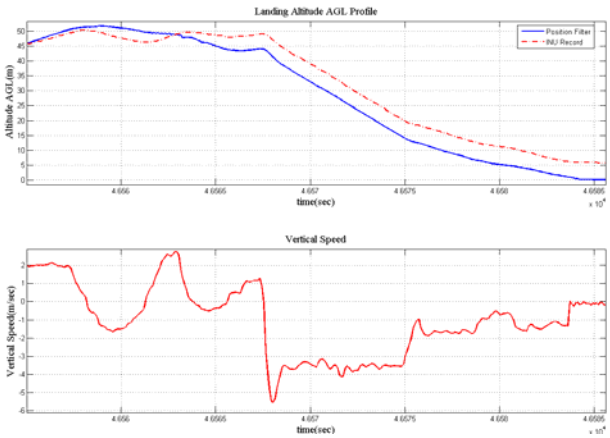

Fig. 7-1. Landing #2

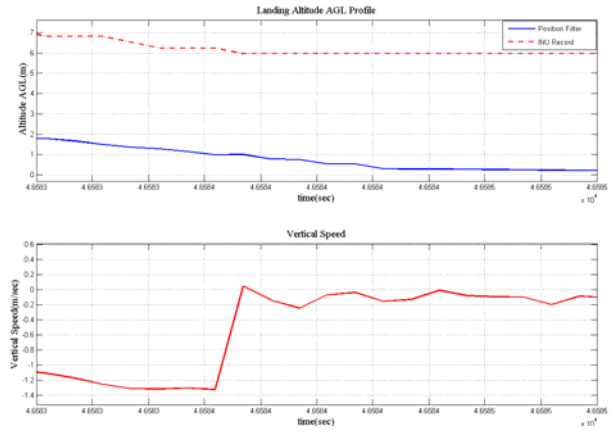

Fig. 7-2. Landing #2 : Close-up View of Touchdown

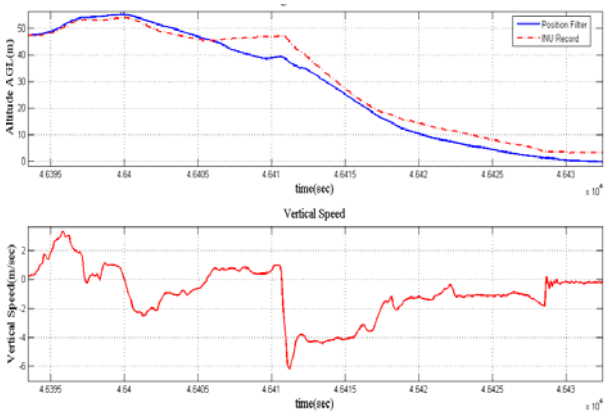

Fig. 8-1. Landing #3

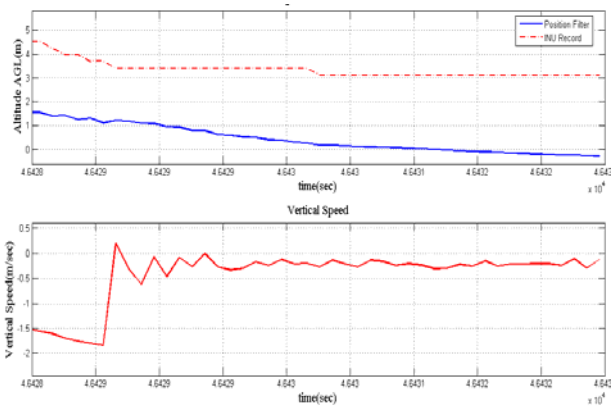

Fig. 8-2. Landing #3 : Close-up View of Touchdown

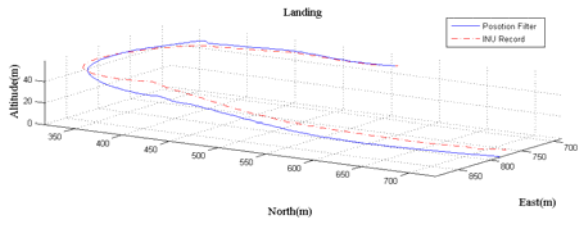

Fig. 9. 3D View of a Landing

6. CONCLUSIONS

In this paper, a vision aided position estimator for autonomous fixed-wing UAV landing was presented. An optical flow estimation algorithm was adopted to add robustness for UAV detection in the vision system. The experiments validated the feasibility of the proposed system and the results are very promising: 50%~80% error reduction in altitude AGL compared to the altitude estimation by a high fidelity INU. The uncertainties in the rover position and camera angles, measurement delay, and the weak observability of the monocular camera are believed to be the main source of errors in the position estimates, and are topics for further investigation. The authors plan to conduct additional experiments including fully autonomous closed-loop landing.

REFERENCES

Brown, R. G. & Hwang, P. Y. C. (1997) *Introduction To Random Signals and Applied Kalman Filtering with Matlab Exercises and Solutions*, John Wiley & Sons, Inc.

Cohen, C. E., Cobb, H. S., Lawrence, D. G., Pervan, B. S., Power, J. D., Parkinson, B. W., Aubrey, G. J., Loewe, W., Ormiston, D., McNally, B. D., Kaufmann, D. N., Wullschleger, V. & Swider, R. J., JR (1995) Autolanding a 737 Using GPS Integrity Beacons. *Navigation : Journal of The Insititute of Navigation,* 42.

Grewal, M. S. & Andrews, A. P. (2001) *Kalman Filtering: Theory and Practice Using MATLAB*, John Wiley & Sons, Inc.

Green, W. E., Oh, P. Y., Sevcik, K. & Barrows, G. (2003) Autonomous Landing for Indoor Flying Robots Using Optic Flow. *ASME International Mechanical Engineering Congress.* Washington, D.C.

Horn, B. K. P. & Schunck, B. G. (1981) Determining Optical Flow. *Artificial Intelligence,* 17**,** 185-203.

Hubbard, D., Morese B., Theodore, C., Tischler, M. & McLain, T. W. (2007) Performamance Evaluation of Vision-Based Navigation and Landing on a Rotorcraft Unmanned Aerial Vehicle. *IEEE Workshop on Applications of Computer Vision.*

Ippolito, C. & Al-Ali, K. (2007) Topological Constructs for Automatic Reconfiguration of Polymorphic Control Systems. *AIAA Inforech@Aerospace.* Sonoma, CA.

McCane, B. & Novins, K. (2001) On Benchmarking Optical Flow. *Computer Vision and Image Understanding,* 84**,** 126-143.

Pisanich, G. & Morris, S. (2002) Fielding an amphibious UAV : development, results and lessons learned. *Digital Avionics Systems Conference.*

Proctor, A. A. & Johnson, E. N. (2005) Vision-only Approach and Landing. *AIAA Guidance, Navigation, and Control Conference and Exhibit.* San Francisco, CA.

Quigley, M., Barber, B., Griffiths, S. R. & Goodrich, M. A. (2005) Towards Real-World Searching with Fixed-Wing Mini-UAVs. *IEEE International Conference on Intelligent Robots and Systems.* Alberta, Canada.

Schultz, H. W., Buschmann, M., Kryger, L., Winkler, S. & Vorsmann, P. (2007) Towards Vision-Based Autonomous Landing for Small UAVs-First Experimental Results of the Vision System. *Journal of Aerospace Computing, Information, and Communication,* 4**,** 785-797.

Tomczyk, A. & Gruszecki, J. (1999) Preliminary Project of the Autonomous Landing System for Unmanned Aircraft. *World Aviation Conference.* San Francisco,CA.